Journal of Power Sources 232 (2013) 246–253

Contents lists available at SciVerse ScienceDirect

Journal of Power Sources

journal homepage: www.elsevier.com/locate/jpowsour

Covalent vs. non-covalent redox functionalization of C–$LiFePO_4$ based electrodes

L. Madec [a], B. Humbert [a], B. Lestriez [a], T. Brousse [a], C. Cougnon [b], D. Guyomard [a], J. Gaubicher [a,*]

[a] Institut des Matériaux Jean Rouxel (IMN), Université de Nantes CNRS, 2 rue de la Houssinière, BP 32229, 44322 Nantes Cedex 3, France
[b] Laboratoire MOLTECH Anjou, UMR-CNRS 6200, Université d'Angers, 2 boulevard Lavoisier, 49045 Angers, France

HIGHLIGHTS

- We functionalize fast redox molecular relay on carbon additive and C–$LiFePO_4$.
- We correlate FTIR, XPS, elemental analysis, dc conductivity and electrochemistry.
- Conductivity is more impacted by covalent molecular grafting than by non-covalent.
- Simultaneous anion and cation based electrochemical processes occur.
- π–π stacking redox grafting does not show adverse effect on Li insertion in C–$LiFePO_4$.

ARTICLE INFO

Article history:
Received 18 July 2012
Received in revised form
9 October 2012
Accepted 29 October 2012
Available online 18 January 2013

Keywords:
Pyrene
Diazonium
Redox functionalization
Carbon additive
$LiFePO_4$
Power performance

ABSTRACT

During high rate utilization of porous Li battery, Li^+ refuelling from the electrolyte limits the discharge kinetics of positive electrodes. In the case of thick electrodes a strategy to buffer the resulting sharp drop of Li^+ concentration gradient would be to functionalize the electrode with anionic based redox molecules (RMR) that would be therefore able to relay intercalation process. The occurrence of these RMR in the electrode should not however, induce adverse effect on Li intercalation processes. In this respect, this work studies the effect of functionalizing LFPC based electrodes by either covalent or non-covalent chemistry, on Li intercalation kinetics. To do so, model molecules containing a nitro group were introduced at the surface of both carbon conducting additives and active material (C–$LiFePO_4$). It is shown that presumably due to formation of sp^3 defects, covalent anchoring using diazonium chemistry inhibits the intercalation kinetics in C–$FePO_4$. On the contrary, if molecules such as pyrene derivatives are immobilized by pi-staking interactions, Li intercalation is not impeded. Therefore non-covalent functionalization of pyrene based RMR appears as a promising route to relay Li intercalation reaction during high power demand. The framework for future development of this strategy is discussed.

1. Introduction

Lithium (Li)-ion batteries are known to deliver relatively high energy densities (150–200 Wh kg^{-1}) in comparison to other electrochemical energy storage systems. This property is associated with redox reactions that take place within the volume of active grains by simultaneous ions and electrons uptake/removal. When low electronic and ionic conductivities materials are involved, high rate can be reached by reducing transport length as in nanograins [1–3] or nanostructured materials [4]. Recent calculations also point out that statistical crystal defects significantly impede Li^+ diffusion constant. Kinetics therefore depends on the lithium diffusion length with microscopic crystals being much favoured than nanoparticles [5]. When fast electronic and ionic motion may occur within the active material, power performance (1–3 kW kg^{-1}) are usually frustrated by slow ionic "refuelling" from the electrolyte [6,7] because the amplitude of intercalation reactions is large in respect to the amount of ions available in the porosity of the electrodes. As the discharge rate increases, bulk Li^+ intercalation processes become surface limited in these parts of the electrode where Li^+ depletion occurs. Therefore for power applications, electrodes are made thin to reduce ionic diffusion path lengths. This results however, in low energy batteries (Wh cm^{-2}). One possible alternative to decreasing the electrode thickness would be to use additional redox molecular relay (RMR) which charge compensation occurs with anions rather than Li^+ ions. This strategy

* Corresponding author. Tel.: +33 (0)2 40 37 39 32; fax: +33 (0)2 40 37 39 95.
E-mail address: joel.gaubicher@cnrs-imn.fr (J. Gaubicher).

0378-7753/$ – see front matter © 2013 Elsevier B.V. All rights reserved.
http://dx.doi.org/10.1016/j.jpowsour.2012.10.100

should therefore not only allow buffering power properties of thick electrodes but also provides means against over discharge/charge issues, considering RMR can be chosen with a redox potential lower (higher) than the active material on discharge (charge). To prevent any dissolution of RMR in the electrolyte of Li-ion batteries, RMR can be functionalized at the active material and/or conducting agent surfaces. However, one should verify that functionalization does not hinder Li^+ intercalation kinetics. This is the main goal of the present study.

So far, molecular functionalization of Li battery components has been proposed to stabilize the SEI (solid electrolyte interface) at the surface of carbon [8], to maintain contact between silicon particles and graphite flakes or carbon nanotubes [9], and to increase cycle life by limiting electrolyte decomposition at the surface of positive active material [10]. Moreover, in the field of electrochemical capacitors, molecular functionalization of carbon has been used to provide a novel type of electrical double layer [11] and to increase energy densities [12–18]. All these works refer however, to covalent functionalization. On the contrary, interest of non-covalent interactions such as π–π staking has only be proven very recently in the field of energy storage [19].

Covalent modification of carbon surface is mostly performed by electrochemical or spontaneous reduction of diazonium salts [20–22]. It occurs along with N_2 departure at a potential threshold close to 0 V vs. SCE (~3 V vs. Li^+/Li^0), leaving an aryl radical that covalently bonds to the surface of the substrate. Among diazonium salts, the para-nitrobenzene derivative is often used as a model molecule because the nitro group can easily be detected from conventional spectroscopies.

This study deals with the functionalization aspects of the carbon additive and the active material of a composite electrode by model RMR chosen as para-nitrobenzene or 1-NitroPyrene. This paper aims at determining first, what can be expected in term of capacity gain from the RMR strategy where the carbon additive and/or on the active material of a composite electrode are functionalized, and second, how covalent or non-covalent functionalization chemistries impact Li intercalation processes.

2. Experimental

2.1. Materials

Carbon coated $LiFePO_4$ powder (referred to as LFPC), with 150 nm particle size, was supplied by UMICORE Cobalt & Specialty Materials, Belgium. Purity (Li = 4.4 wt%, Fe = 34.4 wt%, P = 17.6 wt %) and carbon content (2.8 wt%) were confirmed by XRD and elemental analysis (Service Central d'Analyse–CNRS, Vernaison, France) respectively.

Covalent functionalization of carbon substrates was performed by direct contact of amorphous carbon black Super P, referred to as Csp, or, graphitised carbon black C-NERGY™ Super C65 from TIMCAL, referred to as C65, with dissolved para-nitrobenzene diazonium tetrafluoroborate ($C_6H_4N_3O_2BF_4$, CAS 456-27-9, referred to as PNBDiaz) in ultra pure water (pH = 5–6). In the case of LFPC a similar procedure was followed except PNBDiaz was dissolved in anhydrous acetonitrile (HPLC grade). We shall recall for the sake of clarity that reaction of PNBDiaz at a carbon surface yields the grafting of the para-nitrobenzene moiety ($C_6H_4NO_2$, referred to as PNB) [22]. Non-covalent anchoring was conducted by immersion of C65 in a methanol solution of 1-nitropyrene ($C_{16}H_9NO_2$, CAS 5522-43-0, referred to as NPyr). Taking L as the theoretical amount corresponding to a dense monolayer coverage of PNB at the surface, the amount of PNBDiaz was varied from n = 0.05L to n = 10L for Csp, while it was set to 0.1L and 2L for C65, and 2L for LFPC. Non-covalent functionalization of NPyr was performed for n = 4L in the case of C65. Theoretical dense monolayer coverage was estimated based on Van Der Waals bond distances from the gyration surface area of a grafted phenyl unit in the case of PNB (close to 25 $Å^2$), from the geometrical surface of a pyrene unit (195 $Å^2$) for NPyr, and from specific surface areas deduced from BET analysis for LFPC (23 $m^2\ g^{-1}$), Csp (66 $m^2\ g^{-1}$) and C65 (63 $m^2\ g^{-1}$). The contact time was 24 h and 120 h in case of covalent and non-covalent grafting respectively. The mass powder to solvent volume ratio was held constant (250 mg/16 ml). Grafted Csp, C65 and LFPC samples are referred to as Csp-NO_2-nL, C65-NO_2-nL, C65-PyrNO_2-nL and LFPC-NO_2-nL respectively. All filtered samples were washed three times by a few minutes immersion in 250 ml of ethanol to remove un-grafted species.

2.2. Physical characterizations

Elemental analyses were performed by ICP at Service Central d'Analyse–CNRS, Vernaison, France.

BET surface area analyses were performed with a micromeritics ASAP 2010 apparatus using nitrogen gas.

Fourier transform infrared spectroscopy (FTIR) spectra were collected with a Brucker Vertex 70 in absorbance mode using KBr pellets and a DTGS detector at a resolution of 4 cm^{-1}. KBr was used as a reference and for each samples, 0.2 mg of powder was mixed with 300 mg of KBr.

X-ray photoelectron spectroscopy (XPS) was performed with a Kratos Axis Ultra spectrometer using an Al Kα monochromatic beam working at 1486.6 eV. Data were collected at room temperature and the operating pressure in the analysis chamber was kept below 8 10^{-9} Torr. Powders were deposited onto a carbon tape and all spectra were recorded in the CEA (constant analyser energy) mode with an analyser pass energy of 20 eV. Data treatment was performed with CasaXPS software. To determine the atomic concentrations (in %), pseudo-voight function constrained by full width at half-maximum (FWHM) ranges typical of each element have been used and all spectra are calibrated taking 284.5 eV (graphite like carbon) as a reference binding energy.

2.3. Electrochemical cell preparation and standard cycling protocol

Electrodes constituted of 70 wt% of C, 25 wt% LFPC and 5% of PTFE are referred to as "carbon rich electrodes" where those obtained from 10 wt% of C, 85 wt% LFPC and 5% of PTFE are referred to as "practical electrodes". These mixtures were hand mixed and resulting self supported films were pressed at 5 Tons on a 0.8 cm^2 Al current collector. For both types of electrodes, loadings were close to 15 $mg_{electrode}\ cm^{-2}$ which is a reasonable value for extrapolating electrode performance in a real device [23]. Electrolyte (LP30) obtained from Novolyte as a highly purity grade is 1 M $LiPF_6$ in 1:1 EC-DMC and was used as received. Karl Fischer titration indicates LP30 contains approx. 10 ppm of H_2O. Electrochemical tests were evaluated at 22 °C and monitored by voltammetric potentiostat (VMP-Biologic SA, Claix, France) in galvanostatic mode using EC-Lab software (Biologic SA, version 10.18). All voltages given in the text are reported vs. Li^+/Li^0. Carbon rich electrodes were used in Section 3.3.1 to evaluate the RMR electrochemical behaviour. According to a standard protocol, cycling was performed at a 1 C rate (1Li/1 h, approx. 0.64 mA cm^{-2} or 42.5 mA $g^{-1}_{electrode}$) both on discharge and on charge, in a 3 V or 1.5 V–4.2 V potential range. A 1 min open circuit voltage (OCV) was allowed upon each half cycle. In Section 3.3.2, practical electrodes were used to study the power capability of LFPC based functionalized electrodes. Power tests were performed by successive discharge current pulses of decreasing values after three cycles at a C/5 rate. OCV relaxations

periods were applied in between each current pulse until dE/dt = 1 mV h^{-1}.

3. Results and discussion

3.1. Theoretical capacity gain from redox grafting battery electrodes

Considering a practical battery electrode containing 85 wt% active material, 10 wt% carbon and 5% wt binder, the surface of the carbon additive and of LFPC is unused in terms of faradic process. Therefore, functionalization of this surface by RMR appears as a possible path toward performance optimization, especially at high cycling rate where fast RMR are expected to relay slow bulk Li-intercalation processes. Because of the Li^+ depletion occurring within the electrode porosity, this relay effect is expected to be more pronounced (that is to say the capacity ratio Q_{RMR}/Q_{LFP} should increase) if the electrochemical activity of RMR does not rely on Li^+ ions. For such electrodes, the gravimetric capacity (n mAh $g_{electrode}^{-1}$) associated with functionalized components is Q_{RMR} (mAh g_{RMR}^{-1}) times the weight % of RMR within the electrode. For such electrodes, the gravimetric capacity (n mAh $g_{electrode}^{-1}$) depends on the surface area of the substrate and on the surface density, Γ, of RMR. Fig. 1 compares the experimental capacity delivered at a 4 C rate by a non-grafted LFPC electrodes of 15 $mg_{electrode}$ cm^{-2} (12.75 mg_{LFP} cm^{-2}, 2.1 mAh cm^{-2} based on 165 mAh g_{LFP}^{-1}) to the theoretical capacity that should be obtained for a composite electrode that contain either functionalized Csp (S_{BET} = 66 m^2 g^{-1}) of functionalized Ketjen black (referred to as KB, S_{BET} = 800 m^2 g^{-1}), and functionalized LFPC (S_{BET} = 23 m^2 g^{-1}) at different Γ values of RMR. Simulations were performed using a model RMR with a specific capacity Q_{RMR} = 505 mAh g_{RMR}^{-1}. In our experimental conditions, the discharge capacity for the blank non-grafted LFPC electrode is 42.5 mAh g_{LFPC}^{-1} at 4 C rate (see Section 3.3.2). On this basis, simulation results in substantial capacity gains as Γ increases (Fig. 1).

Although, Csp-RMR brings lower theoretical capacity gain than KB-RMR (Fig. 1) Csp was chosen for the following experimental study because it could be compared to the graphitized C65 carbon with a similar BET surface but that allows non-covalent π stacking

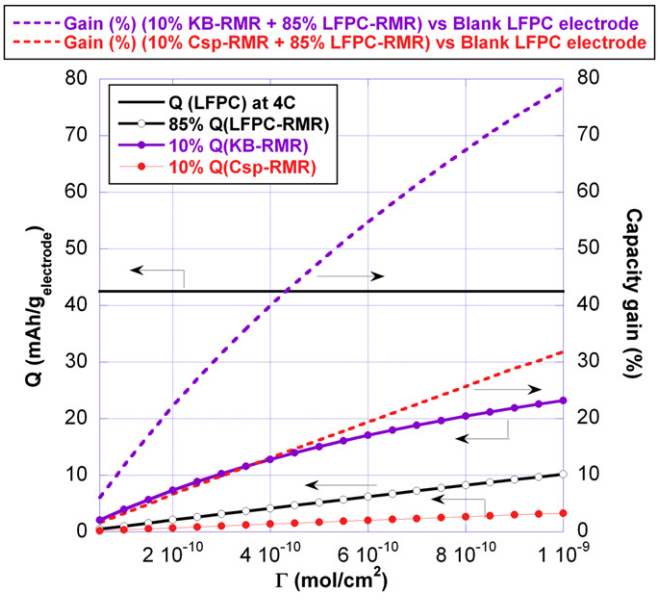

Fig. 1. Variation as a function of Γ, of the gravimetric capacity at a 4C rate for model RMR (505 mA h g_{RMR}^{-1}) functionalized on Csp (Csp-RMR), KB (KB-RMR) and LFPC (LFPC-RMR) vs. a blank electrode with 85 wt% of un-grafted LFPC.

of pyrene derivative. Furthermore, because graphitized domains at the surface of LFPC are too small, non-covalent functionalization by π-stacking interactions resulted in very low surface coverage. Therefore, the following experimental section deals with functionalization of Csp and LFPC by covalent chemistry only, and functionalization of C65 by both covalent and non-covalent chemistries.

3.2. Physical characterization of molecular modifications

Fig. 2 shows the FTIR spectra of Csp-NO_2-nL, C65-NO_2-nL and LFPC-NO_2-nL samples. Vibration frequency of relevant molecular groups are gathered in Table 1. It should be noticed that the ratio between the Csp^2 (C=C) bond stretch at 1590 cm^{-1} and the signal corresponding to the COOH group at 1640 cm^{-1} is higher in the case of C65 (Fig. 2C-a) compared to Csp (Fig. 2A-a). This result, in agreement with the XPS C1s core peaks spectra (not showed) confirms C65 is more graphitized than Csp. For Csp-NO_2-nL and C65-NO_2-nL, growing antisymmetric and symmetric stretching bands related to NO_2 moieties are detected at 1520 cm^{-1} and 1340 cm^{-1} as nL increases from 0.05L to 10L and 0.1L to 2L respectively. For LFPC-NO_2-2L, NO_2 groups could also be evidenced at the same frequencies. The frequency difference between antisymmetric and symmetric stretching $\nu_{as} - \nu_s$ = 180 cm^{-1}, lies only slightly above the 159–177 cm^{-1} range reported for solids [24]. Similarly, increasing C=C bond stretching mode of aromatic ring appears at 1590 cm^{-1} for Csp-NO_2-nL and C65-NO_2-nL while for LFPC-NO_2-2L, it could be detected at 1630 cm^{-1} and 1600 cm^{-1}. Most importantly, the stretching vibration band of the N_2^+ diazonium group (2300–2150, not showed) of PNBDiaz could not be observed whatever the substrates and nL were, confirming that all PNBDiaz have reacted or have been removed during washing. All nitro groups are therefore ascribed to functionalized PNB moiety. In the case of C65-PyrNO_2-4L, however, the NO_2 group of NPyr could not be detected in the 1550–1300 cm^{-1} region although the typical signature of pyrene units is observed between 900 cm^{-1} and 650 cm^{-1} (Fig. 3). We note that these bands are slightly shifted toward higher frequencies, suggesting the occurrence of interactions with substrate. We believe NO_2 bands are not observed due to specific configuration of NPyr at the carbon surface. Indeed, considering a planar geometry for NPyr, a minimum energy is expected for chemisorptions parallel to the graphitic plan. Accordingly, an electrical dipole opposite to that of NO_2 groups may be induced. This would therefore strongly decrease the moment IR transition, and thus, its FTIR signal. DFT calculations are in progress to verify this hypothesis. Raman spectroscopy was attempted to detect NO_2 groups. However, presumably because of strong Raman resonance signals and strong visible absorption of the nano-carbon material, signals were too weak to be observed.

Semi-quantitative XPS analyses were conducted to quantify molecular coverage Γ of Csp-NO_2-nL, C65-NO_2-nL and LFPC-NO_2-nL. XPS binding energy of relevant molecular groups are reported in Table 1. Corresponding N1s core peaks spectra are reported on Fig. 2. In the case of Csp-NO_2-nL (Fig. 2B), several N1s peaks are observed depending on nL whereas nitrogen is not detected for control samples (blank). For nL < 0.2, a single N1s peak is detected at approx. 405.8 eV as expected for NO_2 groups. We note that for nL > 0.2, a small additional N1s peaks which intensity is nearly constant with nL, is observed at approx. 407.2 eV. The origin of this peak is still uncertain. At 400.4 eV however, a double peak appears more and more pronounced as nL increases. It is assigned to azo bridge (Aryle-N=N-Aryle) arising from multilayer stacking of phenyl units in meta position [25,26]. Other authors ascribed these peaks to the reduction of NO_2 groups by the X-ray beam [27]. From our results and in agreement with the findings of Downard [28], this hypothesis is unlikely in our case as peak

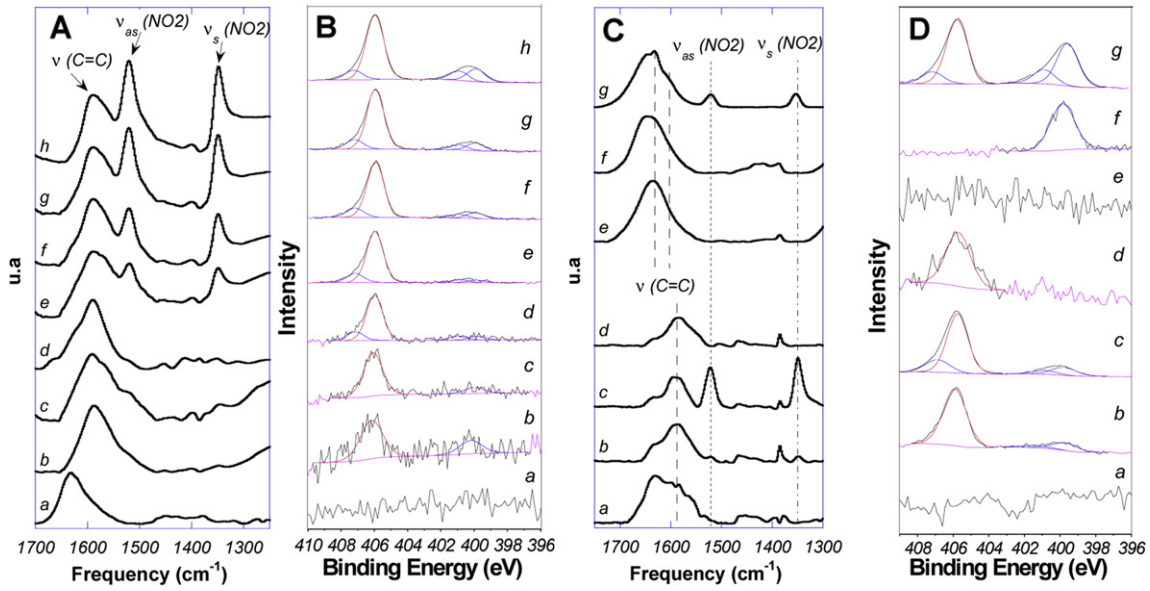

Fig. 2. FTIR spectra of (A) (a) Csp-blank, (b) Csp-NO_2-0.05L, (c) Csp-NO_2-0.1L, (d) Csp-NO_2-0.2L, (e) Csp-NO_2-0.5L, (f) Csp-NO_2-1L, (g) Csp-NO_2-2L, (h) Csp-NO_2-10L and (C) (a) C65-blank, (b) C65-NO_2-0.1L, (c) C65-NO_2-2L, (d) C65-PyrNO_2-4L, (e) LFPC (f) LFPC-blank and (g) LFPC-NO_2-2L. Evolution of N 1s core peaks for (B) (a) Csp-blank, (b) Csp-NO_2-0.05L, (c) Csp-NO_2-0.1L, (d) Csp-NO_2-0.2L, (e) Csp-NO_2-0.5L, (f) Csp-NO_2-1L, (g) Csp-NO_2-2L, (h) Csp-NO_2-10L and (D) (a) C65-blank, (b) C65-NO_2-0.1L, (c) C65-NO_2-2L, (d) C65-PyrNO_2-4L, (e) LFPC (f) LFPC-blank and (g) LFPC-NO_2-2L.

intensity remains unchanged all along data collection. NO_2 functionalization of both C65 and LFPC is also confirmed by a similar evolution of the N1s peaks in the 406 eV and 400 eV regions (Fig. 2D). We note that in the case of LFPC, an additional peak is detected at 399.8 eV both for the blank sample (LFP immersed in acetonitrile without PNBDiaz), and for the grafted sample. It is not however, detected for the raw LFPC powder before immersion. This peak is therefore ascribed to adsorbed acetonitrile molecules that could not be removed upon washings (see Experimental section). For the three samples, characteristic peaks of diazonium N_2^+ moiety (402–405 eV range [29]) are not observed in agreement with FTIR results. This point is further supported by the absence of boron in the 192 eV region which would have been associated with BF_4^- counter anions of unreacted PNBDiaz. As expected, in the case of C65-PyrNO_2-4L, the N1s core spectrum only shows the signal associated with the NO_2 group.

PNB coverage (Γ_{chem}) was derived thanks to the NO_2 chemical probe. To do so, the N_{NO2}/N_{total} atomic ratio obtained from XPS semi-quantitative analysis was multiplied by the weight % of N_{total} determined from elemental analysis (referred to as El-Ana) (Table 2). Resulting Γ_{chem} are reported in Table 2 and on Fig. 4 in wt% as well as in mol cm^{-2} on the basis of the BET surface area. In the case of Csp-NO_2-nL, results clearly show that the surface coverage tends to saturate for nL > 2L at Γ_{chem} ~5.1 10^{-10} mol cm^{-2}. Interestingly the value related to LFPC-NO_2-2L is larger (Γ_{chem} ~7.8 10^{-10} mol cm^{-2}, 2.17 wt%) than those associated with the two carbon substrates Csp and C65. Finally, because functionalization with NPyr has been conducted for a period of time (120 h) considered as infinite, pyrene anchors lead to saturation limit of Γ_{chem} ~0.9 10^{-10} mol cm^{-2} which is consistent with our previous results [19].

Table 1
FTIR vibration frequency and XPS binding energy of relevant molecular groups.

Groups	ν (cm^{-1})	BE (eV)
NO_2	1550–1300	405.8
C=C	1590	
Pyrene	900–650	
N_2^+	2300–2150	402–405
N=N		400–401

3.3. Electrochemical characterization of LFPC based functionalized electrodes

Carbon rich electrodes are devoted to the examination of the redox activity of RMR (Section 3.3.1) whereas practical electrodes are used to assess the impact of the covalent or non-covalent grafting chemistry on Li^+ intercalation kinetics in $FePO_4$ (Section 3.3.2). For the sake of clarity, electrochemical tests have only been performed for samples with selected Γ values.

3.3.1. Redox activity of RMR in LFPC based functionalized electrodes

Electrochemistry of nitro group is well documented [28,30–33]: NO_2 groups reduce near 2.0 V to radical anion (eq. (1)) in aprotic media [21] and to hydroxylamine (eq. (2)) and amino species (eq. (3)) in protic media [28]. On charge, radical anion and hydroxylamine are respectively oxidized to NO_2 moiety (eq. (1)) at approx. 2.2 V and to nitroso radical NO° (eq (4)) in the vicinity of 3.2 V. Aminophenyl groups oxidize near 4 V but the corresponding

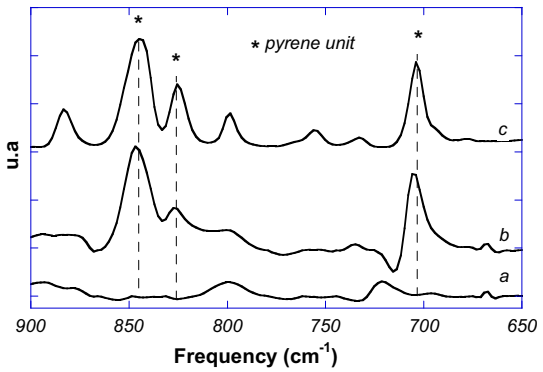

Fig. 3. FTIR spectra of (a) C65-blank, (b) C65-PyrNO_2-4L and (c) NPyr.

Table 2
XPS semi quantitative and elemental analysis results relative to Γ_{chem} for Csp-NO_2-nL, C65-NO_2-nL, C65-PyrNO_2-4L and LFPC-NO_2-2L. *Values are given here precisely as very closed results (less than 5% of difference) was obtained by repeating the grafting and elemental analysis experiments twice. **These values were <0.1% from elemental analysis. They were therefore estimated from the correlation between the wt% determined from El-Ana and the at%(N) determined from XPS for all other samples (not shown). ***This value comes from the physisorbed acetonitrile at the surface of the control LFPC sample (see experimental for details). Accordingly, the at %(N) for the pristine LFPC powder is zero as shown in Fig. 2D-e.

Substrat	Grafting chemistry	Grafted moiety	nL	N_{NO2}/N_{total} (XPS)	N_{total} (wt%) (El-Ana)*	Γ_{chem} (wt%)*	$\Gamma_{chem} \cdot 10^{-10}$ (mol cm^{-2})*
Csp			0	0	0	0.00	0.00
Csp	Covalent	PNB	0.05	0.6	0.09**	0.47	0.58
Csp	Covalent	PNB	0.1	0.78	0.11	0.75	0.92
Csp	Covalent	PNB	0.2	0.74	0.23	1.49	1.85
Csp	Covalent	PNB	0.5	0.77	0.34	2.29	2.84
Csp	Covalent	PNB	1	0.74	0.44	2.86	3.55
Csp	Covalent	PNB	2	0.72	0.65	4.08	5.07
Csp	Covalent	PNB	10	0.68	0.7	4.14	5.14
C65			0	0	0	0	0
C65	Covalent	PNB	0.1	0.75	0.11	0.72	0.93
C65	Covalent	PNB	2	0.68	0.76	4.48	5.82
C65	Π-Stacking	NPyr	4	1	0.08**	1.41	0.90
LFPC			0	0	0.19***	0	0
LFPC	Covalent	PNB	2	0.49	0.51	2.17	7.80

reaction is still unclear [34]. Potentials and amplitudes of these four reactions are summarized on Scheme 1 vs. $Li^+/Li°$ according to Refs. [21] and [28]. The two reversible systems (eqs. (1) and (4)) correspond to gravimetric capacities of 220 and 505 mAh g^{-1} respectively.

$$C_6H_4{-}NO_2 + 1e^- \Leftrightarrow C_6H_4{-}NO_2{}^{\circ -}, \quad U_0 = 2.0\,V \; vs.\; Li^+/Li^0 \qquad (1)$$

$$C_6H_4{-}NO_2 + 6H^+ + 6e^- \rightarrow C_6H_4{-}NH_2 + 2H_2O, \quad U_0 = 2.2\,V \; vs.\; Li^+/Li^0 \qquad (2)$$

$$C_6H_4{-}NO_2 + 4H^+ + 4e^- \rightarrow C_6H_4{-}NHOH + H_2O, \quad U_0 = 2.2\,V \; vs.\; Li^+/Li^0 \qquad (3)$$

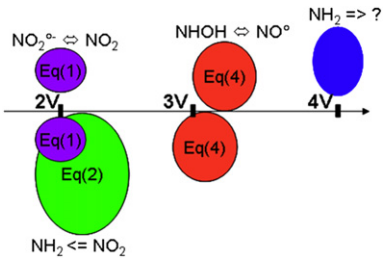

Scheme 1. Depiction of functionalized PNB electrochemistry in protic and aprotic medium.

$$C_6H_4{-}NHOH \Leftrightarrow C_6H_4{-}NO^\circ + 2H^+ + 2e^-, \quad U_0 = 3.2\,V \; vs.Li^+/Li^0 \qquad (4)$$

Incremental capacity and capacity vs. voltage curves are compared with blank ungrafted electrodes in Fig. 5 on first cycle. For the sake of clarity and because electrochemistry of both C65 and Csp blanks as well as Csp-NO_2-0.1L and C65-NO_2-0.1L are very similar, only those relative to C65 are reported. The redox activity of $LiFePO_4$ can be observed in the 3.4–3.7 V region (intense peaks). For both carbon substrates, grafted electrodes shows additional and increasing redox processes with nL, in the vicinity of 2.3 V (referred to as 1) on discharge and, near 3.2 V (referred to as 2) and 3.9 V (referred to as 3) on charge (Fig. 5a). The latter are also detected for C65-PyrNO_2-4L and LFPC-NO_2-2L. Peak 2 corresponds to the NHOH/NO° redox couple (reaction (4)) as reported by Downard [28]. It occurs from approx. 2.5 V–3.60 V simultaneously to Li^+ deinsertion from LFPC. Peak 3 is ascribed to oxidation of grafted aminophenyl moieties [34]. Peak 1 is therefore associated with the transformation of nitro species into both hydroxylamine (reaction (3), $4e^-$) and amino moieties (reaction (2), $6e^-$) with the proton source being the initial traces of H_2O contained in the LP30 (see Experimental section). We did not detect however, the formation of nitro radical anion as in reaction (1). The amount of functionalized nitro species corresponds to that of hydroxylamine and amino moieties. The charge associated with oxidation of hydroxylamine corresponds to the capacity of peak 2 which is a two electron process. The amount of amino species is therefore that of

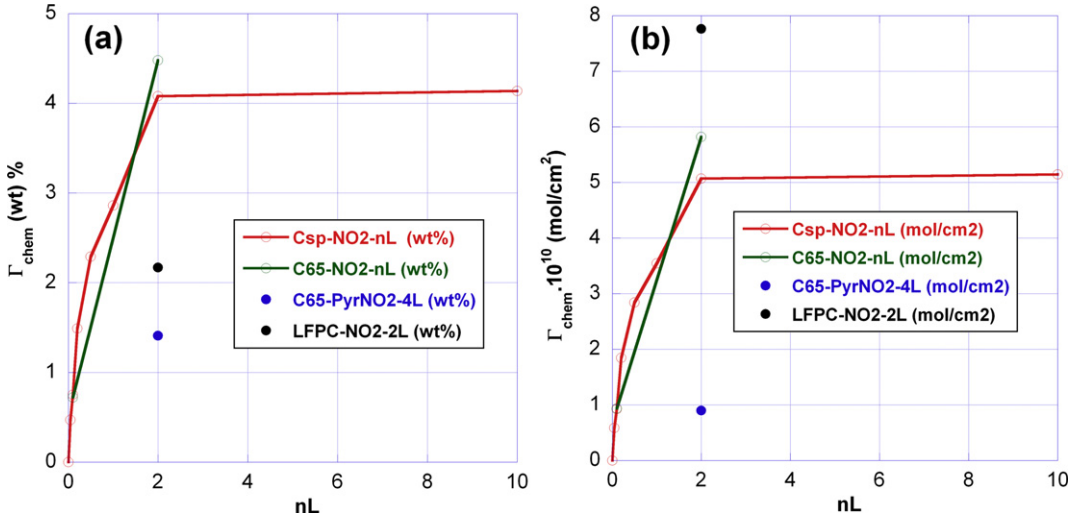

Fig. 4. Evolution of the molecular coverage (a) in wt% and (b) in mol $^{cm-2}$ of Csp-NO_2-nL and C65-NO_2-nL as a function of nL. Values for C65-PyrNO_2-4L and LFPC-NO_2-2L are also reported for the sake of comparison.

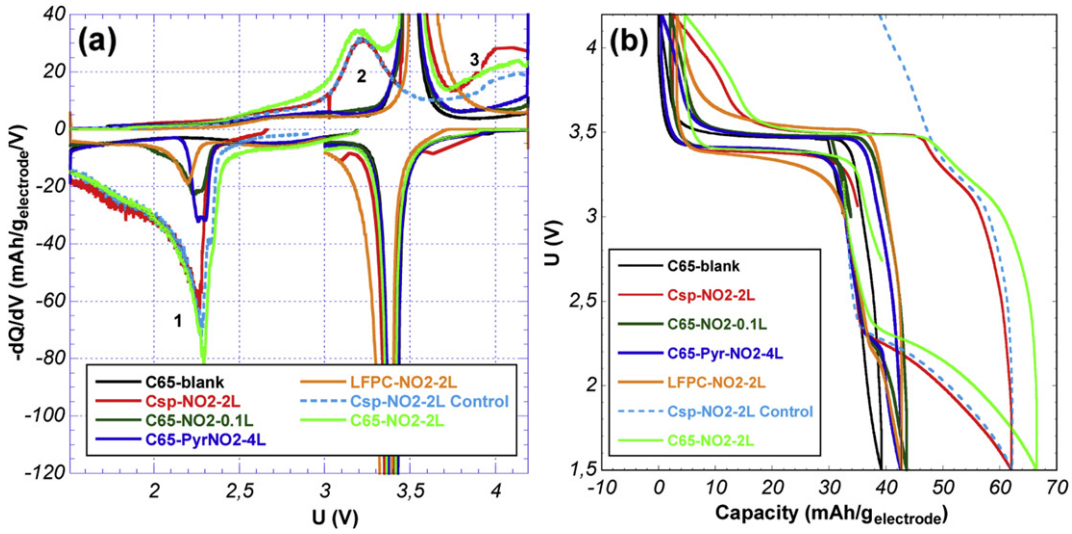

Fig. 5. (a) Incremental capacity curves obtained for carbon rich electrodes based on Csp-NO_2-2L $LFPC^{-1}$, C65-NO_2-nL/LFPC, C65-Pyr-NO_2-4L/LFPC and Csp/LFPC−NO_2−2L at a 1C rate and (b) corresponding variation of the capacity normalized to the whole electrode mass.

peak 1 minus twice that of peak 2. Determination of the capacity of peak 2 is not trivial as part of Li^+ removal from LFPC and oxidation of hydroxylamine moieties occur simultaneously. However, beside LFPC-NO_2-2L, all samples show very close gravimetric capacity and efficiency (vs. theoretical capacity) of Li^+ insertion in LFPC (near 32 mAh $g^{-1}_{electrode}$ and 78% respectively, Table 3). Accordingly, capacities relative to peak 2 has been determined by subtracting that of the blank un-grafted electrode within 2.50−3.60 V. LFPC-NO_2-2L shows lower values due to an evident larger polarization (Fig. 5b). Therefore in that case capacity of peak 2 was determined within 2.5−4 V in order to take into account the larger polarization. We note that the amplitude of peak 2 might therefore be overestimated, which in turn might lead to underestimation of corresponding $\Gamma_{electro}$. Capacity of peak 1 was similarly determined by correction of the blank un-grafted electrode within 2.5−1.5 V. Results are reported in Table 3 together with corresponding surface coverages ($\Gamma_{electro}$) and redox efficiencies ($\Gamma_{electro}/\Gamma_{chem}$*100). Validation of our protocol for data treatment was confirmed by the fair consistency of results obtained for a control electrode that contained 95 wt% of Csp-NO_2-2L and 5 wt% of PTFE (Table 3). Beside C65-PyrNO_2-4L, redox efficiencies are close to maximum indicating the major part of RMR is electrically connected when covalent grafting is involved. In the case of the non-covalent chemistry, the relatively lower redox efficiency could be due to partial dissolution of RMR, poor ionic or electronic access to NO_2 groups, or to a specific configuration of these groups as suggested by FTIR results. Nevertheless, for all functionalized samples, oxidation of $C_6H_4NO^\circ$ groups was found to be nearly irreversible in our cycling conditions. As opposed to persistent type radicals such as TEMPO [35], phenylnitroso radicals that are formed during peak 2, are not sterically protected, and therefore react irreversibly with the electrolyte.

3.3.2. *Power properties of LFPC based functionalized electrodes*

The impact of the grafting chemistry, either covalent or non-covalent, on the efficiency of intercalation processes in LFPC was further examined through power tests of practical electrodes. For this purpose, the potential window was restricted to above the redox activity of nitro groups so that only Li intercalation in LFPC is probed. As shown in Fig. 6a, increasing nL results in a significant decline of the intercalation discharge capacity of covalently grafted carbon and LFPC based electrodes. It is however, very instructive that for same $\Gamma_{electro}$ values, C65 based electrodes are less impacted by covalent functionalization than Csp ones (Fig. 6a). On the contrary, non-covalent functionalization of C65 prevents any alteration of the electrode power behaviour and therefore of Li intercalation kinetics in LFPC. Indeed, for similar $\Gamma_{electro}$ values, C65-PyrNO_2-4L power response is superimposed to that of the blank C65 electrode whereas in the case of C65-NO_2-0.1L the capacity is 27% lower at 4C rate.

For active materials that show relative fast electrical migrations, high rate performance strongly depend on electronic and ion resistances to transport throughout the electrode via respective percolating sub-networks. Voltage drops associated with Li^+ migration, depends on the thickness (L) of the electrode, the porosity (ε), the tortuosity (τ) and on ion injection processes into active grains [7,36]. In the present study, electrode loadings,

Table 3
Gravimetric capacity, corresponding molecular coverage $\Gamma_{electro}$ as well as resulting redox efficiency ($\Gamma_{electro}/\Gamma_{chem}$*100) for Csp-$NO_2$-nL, C65-$NO_2$-nL, C65-Pyr$NO_2$-4L and LFPC-$NO_2$-2L.

Samples	Grafting chemistry	Q_{disch} (LFPC) (mAh $g^{-1}_{electrode}$)	Q (peak 1) (mAh $g^{-1}_{electrode}$)	Q (peak 2) (mAh $g^{-1}_{electrode}$)	$\Gamma_{electro}\cdot10^{-10}$ (mol cm^{-2})	Efficiency (%) LFPC RMR	
Csp-Blank		32.2	0		0	78	0
Csp-NO_2-0.1L	Covalent	32.0	4.3	1.5	0.8	78	86
Csp-NO_2-2L	Covalent	32.8	23.6	11.9	4.8	80	94
Csp-NO_2-2L Control electrode	Covalent		25.3	11.8	5.0		98
C65-NO_2-0.1L	Covalent	31.8	4.3	1.3	0.7	77	80
C65-NO_2-2L	Covalent	31.8	27.3	12.8	5.5	77	93
C65-PyrNO_2-4L	Π-Stacking	32.4	3.4	1.1	0.6	79	68
LFPC-NO_2-2L	Covalent	29.0	4.6	2.1	7.1	70	92

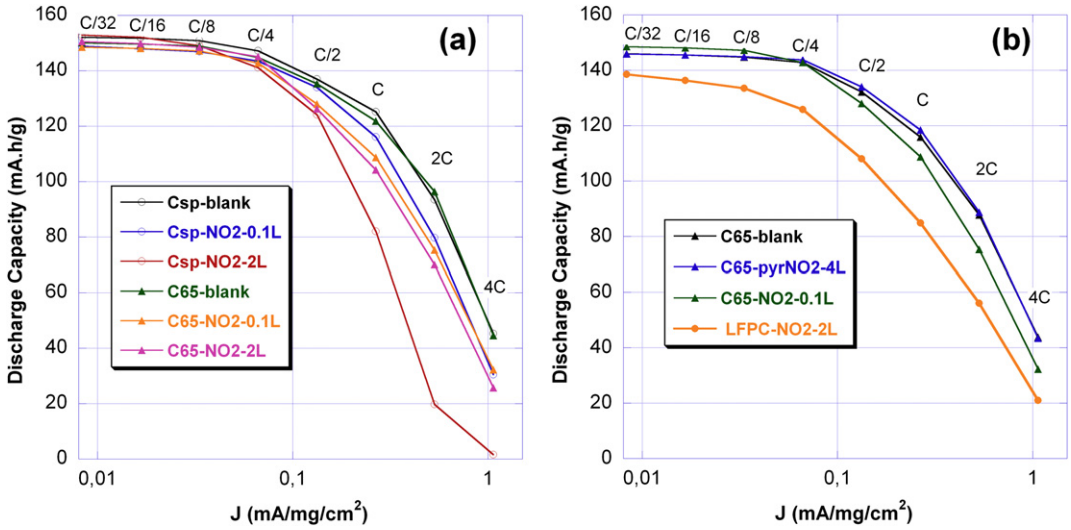

Fig. 6. Signature curves for (a) Csp-NO_2-nL and C65-NO_2-nl, and (b) C65-PyrNO_2-4L and LFPC-NO_2-2L.

(~2.1 mAh cm^{-2}), thickness (90 μm) and porosity (50%) were kept to identical values within a 5% error. Furthermore the electrode preparation including the mixing step was rigorously the same (see Experimental section). Accordingly, ionic effects are expected to be comparable for both blank and grafted electrodes. Voltage drops associated with electronic transport depend on resistances of the carbon coating and of all contacts (involving LFPC clusters, C clusters/binder, and current collector), as well as on the length and number of electronic paths from the current collector to the active material grain. The latter depends on the position of the intercalating LFPC grain within the electrode. Indeed, *operando* XAS mapping have demonstrated important inhomogeneities of composition while discharging LFPC electrodes [37]. Therefore, in the present study such a marked difference in power responses between electrodes based on covalently or non-covalently functionalization can be tentatively assigned to the formation of sp^3 defects that stem from covalent anchoring. Indeed, covalent functionalization or oxidation of carbon substrate results in formation of sp^3 defects that may decrease the electronic conductivity by several order of magnitudes [38–43]. Similarly, sp^3 defects within the carbon coating of LFPC were recently shown to be a major source of electronic conductivity drop [44]. On the contrary, molecular functionalization of carbon substrates by non-covalent interactions, typically π–π interactions, with aromatic ring units such as pyrene molecules, should not result in strong scattering of electron transport [45–47]. Accordingly simultaneous high power and energy performance could be obtained for carbon electrodes functionalized with ferrocene pyrene derivatives [19].

A comparative study of DC conduction at equivalent Γ for the two different grafting chemistries has been performed. Such a study has never been conducted to our knowledge. Two points measurement were performed on pellets containing the same mixture than that used for power tests. Electronic conductivities are $\sigma_e = 0.536$ S m^{-1}, $\sigma_e = 0.502$ S m^{-1} and $\sigma_e = 0.454$ S m^{-1} for C65-Blank, C65-PyrNO_2-4L and C65-NO_2-0.1L respectively. Covalent functionalization therefore introduce a 15% decrease of conductivity whereas the degree of functionalization corresponds to a maximum of 1 molecule anchored per 79 carbon atoms (real value should be lower however, considering diazonium grafting generates multitasking), taking 7.3 10^{-9} mol cm^{-2} as a rough approximation of the carbon density at the C65 surface [48]. On the contrary, non-covalent attachment shows the lowest impact on the electronic conduction with a 6% decrease vs. the C65-Blank. Frequency dependent electrical measurements as well as morphological investigations of the electrode are underway to quantify the contribution of contacts between clusters.

We note that if π–π based functionalization should be preferred in regard of its impact on kinetics if Li intercalation process, they offer a limited ability to extend the molecular coverage above 1.7 10^{-10} mol cm^{-2} [19]. Therefore, the next step is to propose new grafting chemistries that would cumulate both a high degree of functionalization and a low impact on electronic transport through the electrode.

4. Conclusion

As a new approach to address power peak demands of battery electrodes, we suggest a new strategy based on the use of fast redox molecule (RMR) grafted at the surface of electrode components to relay Li-ion insertion processes. This includes functionalization of the carbon additive and the active material. Calculations show that a practical electrode (2.1 mAh cm^{-2}) that contains 10% of Ketjen Black and 85% LFPC both being grafted with practical surface coverage by a RMR of 505 mAh g_{RMR}^{-1} may deliver additional 23 mAh $g_{electrode}^{-1}$ to the capacity associated with Li intercalation in LFPC. In our experimental conditions it represents at a 4 C rate, close to a 50% gain vs. the control non-grafted LFPC electrode. This strategy rely however, on the fact that functionalization does not inhibits Li ion intercalation kinetics. Therefore we have investigated in this work the impact of either covalent or non-covalent functionalization on the electrochemical behaviour of the active material LFPC. To this aim we used either nitrophenyl diazonium salt and 1-nitropyrene derivative. Thanks to the nitro probe, FTIR, XPS, elemental analysis and electrochemical experiments show that covalent anchoring significantly decreases the power ability of Li ion intercalation process presumably due to sp^3 defects. On the contrary, functionalization of the electrode by pyrene derivatives should be favoured because it does not impeded Li intercalation in the active material. So far however, the molecular coverage that can be routinely reached with such π–π interactions is five times lower than that obtained using covalent anchoring. Based on this study, further experiments are presently conducted to demonstrate the occurrence of molecular relay effect in pyrene based functionalized electrodes and to determine its optimal composition. Search for even more effective grafting chemistry is also a key point to be addressed.

References

[1] C. Delacourt, P. Poizot, S. Levasseur, C. Masquelier, Electrochem. Solid State Lett. 9 (2006) A352.
[2] P. Poizot, S. Laruelle, S. Grugeon, L. Dupont, J.-M. Tarascon, Nature 407 (2000) 496.
[3] P.G. Bruce, B. Scrosati, J.M. Tarascon, Angew. Chem. Int. Ed. 47 (2008) 2930.
[4] L.F. Nazar, G. Goward, F. Leroux, M. Duncan, H. Huang, T. Kerr, J. Gaubicher, Int. J. Inorg. Mater. 3 (2001) 191.
[5] R. Malik, D. Burch, M. Bazant, G. Ceder, Nano Lett. 10 (2010) 4123.
[6] P.A. Johns, M.R. Roberts, Y. Wakizaka, J.H. Sanders, J.R. Owen, Electrochem. Commun. 11 (2009) 2089.
[7] C. Fongy, A.C. Gaillot, S. Jouanneau, D. Guyomard, B. Lestriez, J. Electrochem. Soc. 157 (2010) A885.
[8] Q. Pan, H. Wang, Y. Jiang, J. Mater. Chem. 17 (2007) 329.
[9] C. Martin, M. Alias, F. Christien, O. Crosnier, D. Bélanger, T. Brousse, Adv. Mater. 21 (2009) 4735.
[10] F. Tanguy, J. Gaubicher, A.-C. Gaillot, D. Guyomard, J. Pinson, J. Mater. Chem. 19 (2009) 4771.
[11] D. Pech, D. Guay, T. Brousse, D. Bélanger, Electrochem. Solid State Lett. 11 (2008) A202.
[12] K. Kalinathan, D.P. Desroches, X. Liu, P.G. Pickup, J. Power Sources 191 (2008) 182.
[13] R.D.L. Smith, P.G. Pickup, Electrochim. Acta 54 (2009) 2305.
[14] R.D.L. Smith, P.G. Pickup, Electrochem. Commun. 11 (2009) 10.
[15] G. Pognon, T. Brousse, L. Demarconnay, D. Bélanger, J. Power Sources 196 (2011) 4117.
[16] G. Pognon, T. Brousse, D. Bélanger, Carbon 49 (2011) 1348.
[17] Z. Algharaibeh, P.G. Pickup, Electrochem. Commun. 13 (2011) 147.
[18] Z. Algharaibeh, X. Liu, P.G. Pickup, J. Power Sources 187 (2009) 640.
[19] L. Madec, A. Bouvrée, P. Blanchard, C. Cougnon, T. Brousse, B. Lestriez, D. Guyomard, J. Gaubicher, Energy Environ. Sci. 5 (2012) 5379.
[20] M. Delamar, R. Hitmi, J. Pinson, J.-M. Savéant, J. Am. Chem. Soc. 14 (1992) 5883.
[21] P. Allongue, M. Delamar, B. Desbat, O. Fagebaume, R. Hitmi, J. Pinson, J.-M. Savéant, J. Am. Chem. Soc. 119 (1997) 201.
[22] A. Adenier, E. Cabet-Deliry, A. Chausse, S. Griveau, F. Mercier, J. Pinson, C. Vautrin-Ul, Chem. Mater. 17 (2005) 491.
[23] Y. Gogotsi, P. Simon, Science 334 (2011) 917.
[24] R.A. Nyquist, Interpreting Infrared, Raman and Nuclear Magnetic Spectra, vol. 2, Academic Press, New York, 2000, p 173.
[25] M. Toupin, D. Bélanger, J. Phys. Chem. C 111 (2007) 5394.
[26] P. Doppelt, G. Hallais, J. Pinson, F. Podvorica, S. Verneyres, Chem. Mater. 19 (2007) 4750.
[27] C. Combellas, M. Delamar, F. Kanoufi, J. Pinson, F.I. Podvorica, Chem. Mater. 17 (2005) 3968.
[28] S.S.C. Yu, E.S.Q. Tan, R.T. Jane, A.J. Downard, Langmuir 23 (2007) 11074.
[29] P. Brant, R.D. Feltham, J. Organomet. Chem. 120 (1976) C53.
[30] D.H. Geske, A.H. Maki, J. Am. Chem. Soc. 82 (1960) 2671.
[31] J.H. Wagenknecht, J. Org. Chem. 42 (1977) 1837.
[32] A. Adenier, M.-C. Bernard, M.M. Chehimi, E. Cabet-Deliry, B. Desbat, O. Fagebaume, J. Pinson, F. Podvorica, J. Am. Chem. Soc. 123 (2001) 4541.
[33] M. Delamar, G. Désarmot, O. Fagebaume, R. Hitmi, J. Pinson, J.-M. Savéant, Carbon 35 (1997) 801.
[34] J. Lyskawa, D. Belanger, Chem. Mater. 18 (2006) 4755.
[35] A. Olivier, S. Fawzia, G. Christelle, M. Dias, T. Breton, E. Levillain, Chem. Phys. Chem. 10 (2009) 2401.
[36] B. Kang, G. Ceder, Nature 458 (2009) 190.
[37] Ouvrard Guy, Actual. Chim. 356–357 (2011) 52–56;
G. Ouvrard, M. Zerrouki, P. Soudan, B. Lestriez, C. Masquelier, M. Morcrette, S. Hamelet, S. Belin, A.M. Flank, F. Baudelet, J. Power Sources 229 (2013) 16.
[38] C. Klinke, J.B. Hannon, A. Afzali, P. Avouris, Nano Lett. 6 (2006) 906.
[39] L.S. Woo, B.S. Kim, S. Chen, Y. Shao-Horn, P.T. Hammond, J. Am. Chem. Soc. 131 (2009) 671.
[40] D. Pantea, H. Darmstadt, S. Kaliaguine, L. Sümmchen, C. Roy, Carbon 39 (2001) 1147.
[41] K. Balasubramanian, M. Friedrich, C. Jiang, Y. Fan, M. Burghard, K. Kern, Adv. Mater. 15 (2003) 1515.
[42] L. Cai, J.L. Bahr, Y. Yao, J.M. Tour, Chem. Mater. 14 (2002) 4235.
[43] L. Ji, M. Rao, H. Zheng, L. Zhang, Y. Li, W. Duan, J. Guo, E.J. Cairns, Y. Zhang, J. Am. Chem. Soc. 133 (2011) 18522.
[44] K.A. Seid, J.-C. Badot, O. Dubrunfaut, S. Levasseur, D. Guyomard, B. Lestriez, J. Mater. Chem. 22 (2012) 2641.
[45] C. Ehli, G.M.A. Rahman, N. Jux, D. Balbinot, D.M. Guldi, F. Paolucci, M. Marcaccio, D. Paolucci, M. Melle-Franco, F. Zerbetto, S. Campidelli, M. Prato, J. Am. Chem. Soc. 128 (2006) 11222.
[46] D.I. Schuster, J.D. Megiatto Jr., Nat. Chem. 1 (2009) 182.
[47] C. Ehli, C. Oelsner, D.M. Guldi, A. Mateo-Alonso, M. Prato, C. Schmidt, C. Backes, F. Hauke, A. Hirsch, Nat. Chem. 1 (2009) 243.
[48] Yi-Chun Liu, Richard L. McCreery, J. Am. Chem. Soc. 117 (1995) 11254.